ACS APPLIED MATERIALS & INTERFACES

www.acsami.org

Research Article

Transparent Anti-SARS-CoV-2 and Antibacterial Silver Oxide Coatings

Mohsen Hosseini, Alex W. H. Chin, Myra D. Williams, Saeed Behzadinasab, Joseph O. Falkinham, III, Leo L. M. Poon,* and William A. Ducker*

Cite This: *ACS Appl. Mater. Interfaces* 2022, 14, 8718–8727

Read Online

ACCESS | Metrics & More | Article Recommendations | Supporting Information

ABSTRACT: Transparent antimicrobial coatings can maintain the aesthetic appeal of surfaces and the functionality of a touch-screen while adding the benefit of reducing disease transmission. We fabricated an antimicrobial coating of silver oxide particles in a silicate matrix on glass. The matrix was grown by a modified Stöber sol–gel process with vapor-phase water and ammonia. A coating on glass with 2.4 mg of Ag_2O per mm^2 caused a reduction of 99.3% of SARS-CoV-2 and >99.5% of *Pseudomonas aeruginosa*, *Staphylococcus aureus*, and methicillin-resistant *Staphylococcus aureus* compared to the uncoated glass after 1 h. We envisage that screen protectors with transparent antimicrobial coatings will find particular application to communal touch-screens, such as in supermarkets and other check-out or check-in facilities where a number of individuals utilize the same touch-screen in a short interval.

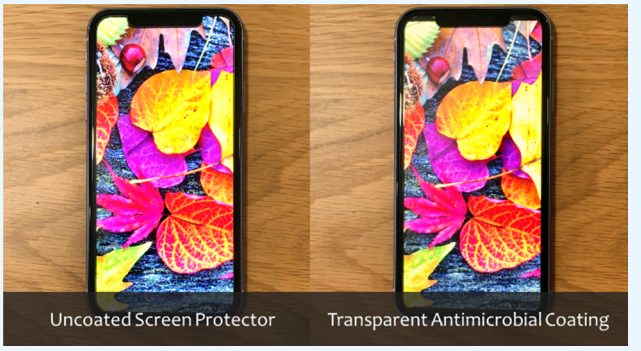

KEYWORDS: *SARS-CoV-2, antibacterial, antiviral, antimicrobial, silver oxide, Ag_2O, transparent, coating, COVID-19*

1. INTRODUCTION

Pathogenic microbes are responsible for a wide variety of diseases. The routes of transmission vary among microbes and depend on a variety of variables[1] such as temperature and climate. Viruses and microorganisms are known to be transmitted through one or a combination of five main routes:[2] (1) direct contact, (2) airborne, (3) droplet, (4) vehicle-borne including via fomites, and (5) vector-borne. Strategies to reduce pathogen transmission can be used to reduce the prevalence of disease in the community and to reduce healthcare-associated infections (HAIs).

Staphylococcus aureus (*S. aureus*), methicillin-resistant *S. aureus* (MRSA), and *Pseudomonas aeruginosa* (*P. aeruginosa*), three common infectious bacteria[3,4] in healthcare settings, cause mild to life-threatening infections that set the stage for maladies such as bloodstream, urinary tract and surgical site infections, sepsis, and pneumonia[3,5] These bacteria are considered a major threat to public health[6,7] and can be transmitted through contaminated fomites.[5,8,9]

The coronavirus disease 2019 (COVID-19) pandemic has dramatically increased the need to control pathogen transfer in different settings. By December 2021, COVID-19 had been responsible for the death of almost more than 5 million people[10] and is known to spread more easily than other coronavirus diseases.[11] Although the main transmission route of severe acute respiratory syndrome coronavirus 2 (SARS-CoV-2), the virus that causes COVID-19, is the inhalation of contaminated respiratory droplets,[12] the transmission modes of this virus are believed to be direct contact, airborne, and contaminated fomites.[13] One modeling study suggested that 25% of transmission is via fomites,[14] and SARS-CoV-2 is known to be stable on a skin model up to 96 h at 22 °C.[15] A recent study showed substantial transfer of this virus from fomites to a skin model.[27]

Hand hygiene is believed to be an effective measure to prevent the microbe transfer through contaminated surfaces,[16] but in a fomite-rich environment, cleaning of hands would need to be very frequent.[17] Therefore, health professionals suggest a combination of hand hygiene[18] and surface disinfection[19,20] to mitigate the risk of these microbe transfers.

A parallel approach to the reduction of infection from fomites is to implement coatings on common-use surfaces[21] that quickly inactivate microbes between users. SARS-CoV-2 can remain viable on solid surfaces up to 7 days,[22,23] and the above-mentioned bacteria are stable on surfaces for months,[24,25] depending on the type of solid and environmental conditions. If these periods were reduced by antimicrobial

Received: October 29, 2021
Accepted: January 14, 2022
Published: February 9, 2022

coatings on common-touch surfaces, the window of transmission could be shortened and the spread of COVID-19 and other microbial diseases could be reduced.

To this end, coatings have been developed to kill bacteria,[8,26,36] or viruses[28] and more recently to inactivate SARS-CoV-2.[29−32] The speed of their action is of great importance; clearly one would like the viability of the surface-adherent microorganisms to be eliminated within minutes or even a shorter time after deposition of the microbe on the solid surface.

Another practical criterion for an antimicrobial coating is retention of the function of the surface after it has been coated. This is our motivation for creating transparent antimicrobial coatings. Transparency is necessary for phone screens, touch-screens at supermarkets and check-in facilities, tablets, windows, etc., and touch-screens are a known pathway for the spread of pathogens. For example, mobile phones are a major pathway for bacteria spread in hospitals.[33,34] Touch-screens at supermarkets, etc., have a series of users in a short time, so it is reasonable that pathogens may be spread by contact at these locations.

The antimicrobial coatings have attracted many researchers in the past few years.[35,37,38] To date all published work on coatings that inactivate SARS-CoV-2 describe opaque coatings.[29−32] Here we describe a novel transparent silver oxide coating capable of accelerating the inactivation of the virus, SARS-CoV-2, as well as rapidly killing the bacteria *S. aureus* and *P. aeruginosa*. The coating killed both methicillin-tolerant *S. aureus* and methicillin-resistant *S. aureus*. The latter, known as MRSA, is an important public health issue. The antibacterial properties of silver oxide have been previously reported in nontransparent coatings for medical implants[39] and on catheters.[40] No damage, change in morphology, or cytotoxic effect has been observed against L929 fibroblast cells[41] or G292 osteoblastic cells,[42] which are mammalian cells. Because of such low cytotoxicity, Ag_2O can be used in wide variety of applications from tooth paste against dental pathogens[43] to its use in wound healing injections,[44] anticancer carrier drugs for skin cancer,[45] and orthopedic[42] and dental tissue regeneration.[46]

To fabricate the transparent coatings we employed a novel binding method based on the Stöber sol−gel process,[47−49] that utilized vapor-phase reactants so that menisci could form and react.[50] Our results indicated that the silver oxide transparent coating caused at least a 99.8% decrease in SARS-CoV-2, MRSA, *S. aureus*, and *P. aeruginosa* in 1 h, and that the resulting coating was transparent and allowed operation of an iPhone touch-screen.

2. MATERIALS AND METHODS

2.1. Materials. 100% Ethanol (EtOH ACS grade), 70% ethanol (Reagent grade), sodium hydroxide beads (NaOH ACS grade), nitric acid (70%, ACS grade), and glass slides (25 × 75 × 1 mm) were purchased from VWR. Silver nitrate 99.9% and ammonium hydroxide (Certified ACS Plus) were obtained from Fisher Scientific. Tetraethyl orthosilicate 99.999% (TEOS) was purchased from Sigma-Aldrich. Deionized (DI) water was from a Milli-Q Reference (MilliporeSigma) water purification system.

2.2. Synthesis of Ag_2O Microparticles. The synthesis of silver oxide micro particles has been previously described elsewhere.[51,52] Briefly, 600 mL of 0.01 M $AgNO_3$ in DI water was stirred while 1200 mL of 0.01 M NH_3 in DI water was added dropwise, and then the mixture was stirred for 10 min. Subsequently, 60 mL of 2 M NaOH was added dropwise. The addition of NaOH caused the solution to darken, demonstrating the synthesis of small Ag_2O particles. The suspension was left for 12 h, during which time the particles precipitated. After precipitation, the particles were washed three times with DI water and then three times with ethanol. Lastly, the supernatant liquid was decanted from the particles and particles were left to dry.

2.3. Fabrication of Transparent Silver Oxide Coatings. Glass slides where cut into 12 × 12 mm pieces and cleaned serially with DI water, 70% ethanol, 6 M nitric acid, and DI water, respectively. These glass pieces acted as the Ag_2O-free, control samples. We prepared two different coatings that differed by the solids loading of Ag_2O particles. The Ag_2O-coating had 5.0 mg/mL Ag_2O powder in suspension (1.2 mg of Ag_2O per mm^2 of glass surface) whereas the 2xAg_2O-coating had 10 mg/mL Ag_2O powder in suspension (2.4 mg of Ag_2O per mm^2 of glass surface). To prepare the transparent silver oxide-coated surfaces, the glass pieces were O_2 plasma-treated at 100 W and a pressure of less than 200 mTorr for 5 min. Immediately after the plasma treatment, 34 μL of a suspension of Ag_2O in 2.8% (v/v) TEOS in ethanol solution was applied on the glass pieces. Substrates were then placed in partially sealed leveled containers to limit evaporation and the self-assembly[53,54] of the particles accordingly. After 2 h, the ethanol was evaporated and samples were transferred to a leveled sealed container in contact with vapors of 8 M DI water in ethanol and 7.62 M ammonia in DI water for 20 h. Next, the samples were heat-treated at 50 °C for 40 min. Lastly, samples were blown with high pressure nitrogen, rinsed upside down in DI water for 10 min, and dried with nitrogen gas. We used cleaned glass and Ag_2O-free TEOS-coatedsamples as controls in the antimicrobial experiments.

2.4. Characterization of Microparticles and Coatings. The X-ray diffraction (XRD) pattern obtained from a Bruker D8 Advance diffractometer (monochromatic Cu Kα X-ray, wavelength = 1.5418 Å) was used to identify the crystal structure of the particles. X-ray photoelectron spectroscopy (XPS; PHI VersaProbe III with a monochromatic Al Kα source of 1486.6 eV) was employed to assess the chemical composition of the surface of the film. Scanning electron microscopy (JEOL JSM-IT500) and atomic force microscopy (Asylum Research 3D MFP) were utilized to examine the coating morphology and roughness, respectively. ImageJ software was employed to obtain the synthesized particle size distribution through SEM images. Surface composition was assessed using electron-dispersive X-ray spectroscopy (Oxford Instruments Ultim Max 100). Optical absorbance and transmittance were measured using an Agilent model 8453 UV−Vis spectrometer. The wettability of the coatings was assessed from the contact angle (First Ten Angstroms FTA125) of 10 μL of DI water.

2.5. SARS-CoV-2 Assay. We have described the 50% tissue culture infective dose ($TCID_{50}$) method for SARS-CoV-2 viability tests in detail elsewhere.[29,30] Briefly, both preparation of the virus stock (Hong Kong index SARS-CoV-2 virus) and assessment of the cytopathic effect utilized Vero E6 cells. These cells were cultured at 37 °C and 5% CO_2 in 2% fetal bovine serum and 1% v/v penicillin−streptomycin added to Dulbecco's modified Eagle medium. The viral transport medium consisted of 0.5% (w/v) bovine serum albumin and 0.1% (w/v) glucose in Earle's balanced salt solution with a pH of 7.4. Control samples and coatings were disinfected with 70% ethanol in water and then dried in air at 37 °C overnight.

The antiviral properties were assessed by placing a 5 μL droplet containing 7.8 log unit $TCID_{50}$/mL of SARS-CoV-2 on the test solid at 22−23 °C and 60−70% humidity, and after a predefined time, the sample was eluted in 300 μL of viral transport medium. The viable virus was then measured using the $TCID_{50}$ assay[55,56] in quadruplicates.[57] Three independently produced solid surfaces were tested for each time point, and the antiviral activity at each time point was obtained based on the reduction of log (virus titer).

2.6. Antibacterial Assay. *Microbial Strains.* The microbial strains employed in this study were *P. aeruginosa* strain DSM-9644, *S. aureus* strain ATCC no. 6538, and a methicillin-resistant *S. aureus* (MRSA) strain MA43300 obtained from the Danville Community Hospital (Danville, VA).

https://doi.org/10.1021/acsami.1c20872
ACS Appl. Mater. Interfaces 2022, 14, 8718−8727

Growth of Microbial Strains. Bacterial strains were grown in 5 mL of Tryptic Soy Broth (TSB, BD, Sparks, MD) to midexponential phase at 37 °C with aeration (60 rpm). Following growth, the purity and identity of the cells in the cultures were verified by streaking bacterial cultures on Tryptic Soy Agar (TSA, BD) and incubating at 37 °C for 48 h and examining colonies for species-specific traits (e.g., pigmentation and surface texture).

Preparation of Microbial Strains for Testing. Grown cells were collected by centrifugation (5000*g* for 20 min), the supernatant medium was discarded, and the cells were suspended in 5 mL of sterile phosphate-buffered saline (PBS) by vortexing for 60 s. Those suspensions were centrifuged (5000*g* for 20 min), the supernatant wash was discarded, and the washed cells were suspended in 5 mL of sterile PBS by vortexing for 60 s. The number of colony-forming units (CFU)/mL of each washed suspension was measured by spreading 0.10 mL (in duplicate) of serial dilutions in PBS on TSA plates.

Measurement of Cell Number. Cell number of PBS suspensions of bacteria was measured as colony-forming units (CFU)/mL of suspension. This measures the number of viable cells, i.e., those cells that are able to grow into a colony. A 10-fold dilution series was prepared for each PBS suspension, 0.1 mL of each dilution was spread on TSA in triplicate, and colonies were counted after 48 h of incubation at 37 °C. If no colonies were present for the least dilution, then we rounded this result up to one colony to enable a log transformation. We set this as the detection limit shown in the figures. Any data point at the detection limit is therefore an upper bound for that measurement.

Measurement of Surface Killing. For each microbial strain, a 10 μL droplet of bacterial cells in PBS suspension was placed on each of three individual Ag_2O-coated or uncoated glass pieces. Immediately after drying, each glass piece was transferred to a separate sterile 50 mL centrifuge tube containing 5 mL of sterile PBS, vortexed at the highest setting for 10 s, and sonicated for 1 min in a Branson model 12 ultrasonic cleaner (Shelton, CT), and the CFU/mL of the suspension was measured as described above. The process was repeated at each time point. CFU counts, corrected for dilution, are in tables in Supporting Information.

2.7. Robustness of Coatings. The United States Environmental Protection Agency (EPA) has a required procedure for the evaluation of antibacterial coatings. We followed their procedure[58] but with some minor modifications. The procedure is described more fully in Supporting Information, but in brief, it consists of repeatedly translating a wet sponge across the coating with a mass of 0.45 kg using a Gardco model D10 V abrasion 214 tester. The main modification to the EPA procedure was to use ethanol, because our main application was for transparent surfaces, such as electronic displays, that are usually cleaned with alcohol solutions.

We further tested the particle attachment strength by sonicating the coatings for 3 min in ethanol. The absorbance spectra of the resulting suspensions were then obtained using UV−vis to evaluate the detachment of the particles.

2.8. Statistics. All experiments were performed in three independent trials. Effects were considered significant when p was near or below 0.05. Linear regression was performed using Excel or MATLAB.

3. RESULTS

3.1. Characterization of Ag_2O Particles. The XRD pattern (Figure 1) of the Ag_2O particles is consistent with the known cubic space group and the previously observed XRD pattern of truncated octahedral silver oxide microparticles.[51,52] SEM image of the particles (Figure 2A) shows a morphology consistent with the literature.[51,52] The mean particle size is 1.5 μm (Supporting Information, Figure S1).

3.2. Coatings Contain Ag_2O at or near the Surface. Our plan was to have the Ag_2O protrude from the silica matrix, such that microbes would come into contact with the Ag_2O surface or dissolved ions. SEM images (Figure 2B−D) are consistent with Ag_2O protruding from the silica matrix and show a uniform distribution of particles. EDS of individual particles shows a 2.5:1 ratio of Ag:O which is similar to a 2:1 ratio expected for Ag_2O (Supporting Information, Table S1). We used XPS, which assays only the top 1 nm or so of the interface, to determine whether the Ag_2O was exposed. The results in Figure 3, which show that the surface has about 9% silver for the Ag_2O-coating and 19% for the 2xAg_2O-coating, verified that the particles were at or near the surface and that the amount of silver at the surface scaled with the amount added to the coating.

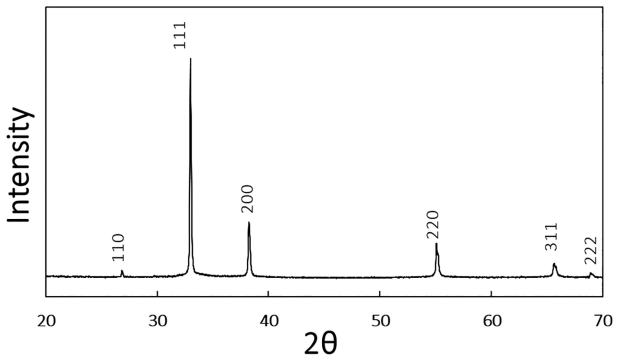

Figure 1. XRD pattern of the Ag_2O particles, which is consistent with the known pattern of Ag_2O microparticles.[51,52] The numbers on each peak indicate the Miller indices of the scattering planes.

The morphology of the particles changed during film formation: the octahedral shape was transformed into lotus-leaf-type features (Figure 2B−D). These features protrude less than about 2 μm from the surrounding silica layer, which has roughness of about 10 nm (see Figure S2). Silver oxide particles are known to have partial solubility when in contact with ammonia[59] or alkali,[60] and the coating was exposed to ammonia vapor during formation. Therefore, the morphology change is a result of a partial dissolution/precipitation process in the presence of ammonia. Figures S4−S6 in Supporting Information show optical time-lapse photography demonstrating that the morphology change is mainly complete after about 12 h, that ammonia is necessary for the reaction, and that the heat treatment does not affect the Ag_2O morphology.

The static contact angles for a 10 μL water droplet on the Ag_2O-coating and the 2xAg_2O-coating were 62 ± 7° and 67 ± 5°, respectively (see Figure S7 in Supporting Information). We also examined how firmly the silver particles were attached to the film by exposing the film to ultrasound while immersed in ethanol for 3 min. We were not able to detect any particles that were removed by ultrasound (see Figure S8 in Supporting Information).

3.3. Silver Oxide Coatings Inactivate SARS-CoV-2. The antiviral activity of transparent silver oxide coatings was evaluated by placing a 5 μL droplet containing SARS-CoV-2 on each coating and measuring the viable virus titer at predefined time points. The results in Figure 4 show that silver oxide coatings are able to greatly accelerate the decay of SARS-CoV-2 compared to the uncoated solid. There are two reference points for considering the effectiveness of the coatings: (1) comparison to the input microbe titer in the test droplet, which we call "inactivation" and (2) comparison to the microbe titer on the uncoated glass at the same time, which we call "*Reduction*", each of which is defined as follows:

https://doi.org/10.1021/acsami.1c20872
ACS Appl. Mater. Interfaces 2022, 14, 8718−8727

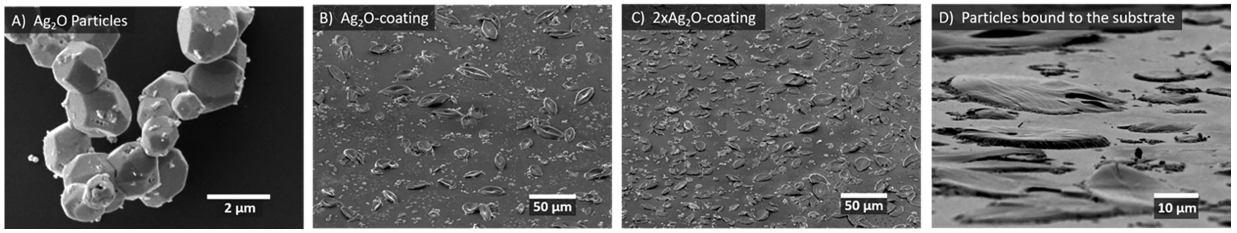

Figure 2. SEM images of (A) Ag_2O particles prior to fabrication of the coating. (B) Ag_2O-coating, (C) $2xAg_2O$-coating, and (D) tilted and magnified view of C. The SEM images show that the coating of particles is uniform and is consistent with Ag_2O protruding from the silica matrix. Additional SEM images of controls are included in Supporting Information, Figure S3.

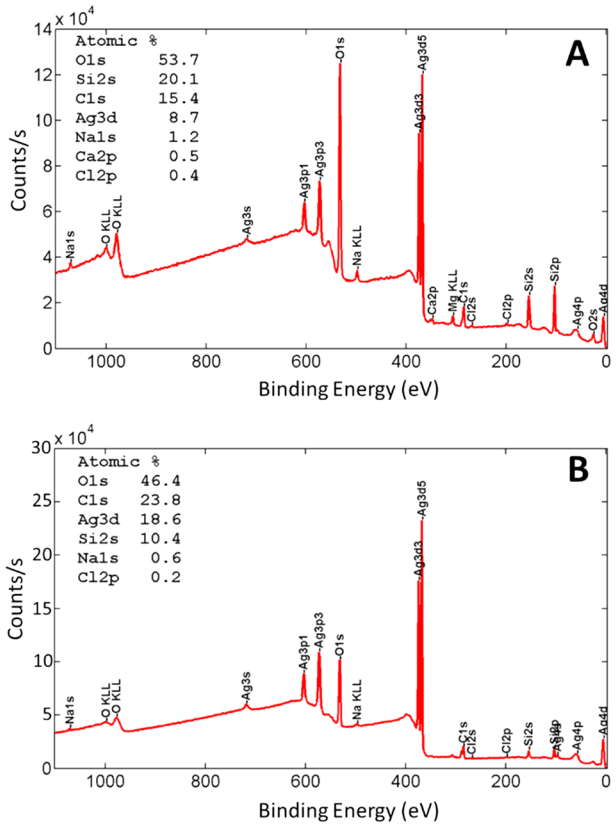

Figure 3. XPS of the silver oxide coatings showing the elemental analysis and confirming the presence of silver and oxygen on the surface. (A) Survey spectrum of the Ag_2O-coating. (B) Survey spectrum of the $2xAg_2O$-coating.

$$\log \text{Inactivation} = \text{mean}[\log_{10}(\text{input titer})] - \text{mean}[\log_{10}(\text{sample titer})] \quad (1)$$

$$\log \textit{Reduction} = \text{mean}[\log_{10}(\text{uncoated titer})] - \text{mean}[\log_{10}(\text{coated titer})] \quad (2)$$

$$\%\ \text{Inactivation} = (1 - 10^{-\log \text{Inactivation}}) \times 100 \quad (3)$$

$$\%\ \textit{Reduction} = (1 - 10^{-\log \textit{Reduction}}) \times 100 \quad (4)$$

In eqs 1 and 2, the titers have been made unitless by multiplying by the volume units, so the same volume units must be used for the two means. The $TCID_{50}$ assay does not measure numbers of virions and instead measures the infectious dose of the virus needed to infect 50% of the tissue culture. The experimental *Reductions* and efficiencies are listed in Table 1. ANOVA (with time and Ag_2O loading as factors) showed that both time ($p = 7 \times 10^{-19}$) and concentration of Ag_2O ($p = 1 \times 10^{-14}$) were significant factors affecting the inactivation of SARS-CoV-2.

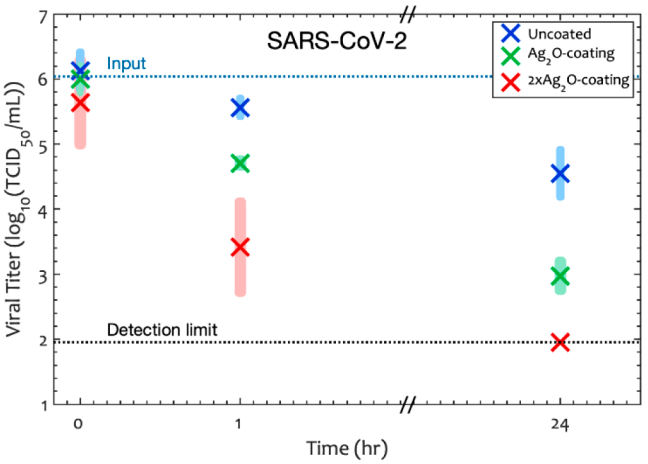

Figure 4. SARS-CoV-2 titer as a function of time and Ag_2O surface density in the coating. Ag_2O-coating has 1.18 mg of Ag_2O per mm^2 of glass surface whereas $2xAg_2O$-coating has 2.36 mg of Ag_2O per mm^2. Shaded rectangles represent the 95% confidence interval calculated only for the points at that condition, and × represents the average of the log of the viral titer at each time point. The results show that the coating inactivates the SARS-CoV-2 virus.

We observed a very slow inactivation of SARS-CoV-2 titer on the uncoated glass: the $TCID_{50}$/mL was decreased by only 66.7% (0.48 $\log_{10}$ reduction) after 1 h. In contrast, on the Ag_2O and the $2xAg_2O$-coatings, the virus was inactivated by 95.4% (1.3 $\log_{10}$ reduction) and 99.8% (2.6 $\log_{10}$ reduction) after 1 h. When we compared the performance of these two transparent coatings with uncoated glass using eq 2 and eq 4, the average *Reduction* was 86.1% for the Ag_2O-coating and 99.3% for the $2xAg_2O$-coating after 1 h. The 95% confidence interval (one tailed, heteroscedastic) indicated that the *Reduction* was more than 73.2% on the Ag_2O-coating and more than 95.7% on the $2xAg_2O$-coating compared to uncoated glass after 1 h. The absence of significant *Reduction* for TEOS-only samples confirmed that silver oxide is the active ingredient for inactivating SARS-CoV-2 (Figure S9 in Supporting Information).

The significance of the silver oxide surface density, c, and time, t, can be determined by a regression analysis. For this analysis we included the zero-Ag_2O (TEOS only)-coating, the Ag_2O-coating, and the $2xAg_2O$-coating. We included a cross-term (tc) because we hypothesized that more SARS-CoV-2 would be inactivated over time if there were a greater density

https://doi.org/10.1021/acsami.1c20872
ACS Appl. Mater. Interfaces 2022, 14, 8718−8727

Table 1. Log Inactivation, Log Survival, and Log Reduction of Microbes after 1 h[a]

	SARS-CoV-2		*P. aeruginosa*		*S. aureus*		MRSA	
Coating	Inactivation	*Reduction*	Survival	*Reduction*	Survival	*Reduction*	Survival	*Reduction*
Ag_2O	1.34	0.86	−4.68	3.79	−2.67	1.77	−2.18	1.44
$2xAg_2O$	2.62	2.15	−4.68	3.79	−3.16	2.26	−3.63	2.89

[a]Inactivation and survival each compare titers to the droplet suspension titer at the time that was used to inoculate the solid. *Reduction* compares to glass at the same time point.

Table 2. Linear Regression Coefficients for Equation 5[a]

		SARS-CoV-2		*P. aeruginosa*		*S. aureus*		MRSA	
Variable	Coefficient	Value	*p*	Value	*p*	Value	*p*	Value	*p*
Constant	*A*	5.904	3×10^{-18}	5.835	10^{-15}	5.709	10^{-19}	6.048	10^{-20}
t	*B*	0.243	0.28	0.014	0.07	0.008	0.07	0.006	0.16
tc	*D*	0.923	1×10^{-6}	0.018	1.9×10^{-4}	0.011	2.3×10^{-4}	0.015	3.5×10^{-6}

[a]*C* was omitted because it was not significant for any microorganism. The small *p* values for *D* show that the half-life of all the microorganisms decreases with concentration of silver oxide in the coating. The linear regression was run with *t* in units of hours and *c* in units of mg/mm^2. For SARS-CoV-2, only the 0 h and 1 h data were included because all the data for the $2xAg_2O$ beyond 1 h was below the detection limit, so only the upper bound was known.

of Ag_2O in the coating. The regression equation has the following form:

$$\log[\mathrm{TCID}_{50}/\mathrm{mL}] = A - Bt - Cc - Dtc \quad (5)$$

where *A*, *B*, *C*, and *D* are coefficients to be determined from the regression. A regression analysis using 0 and 1 h data points showed that $p = 0.12$ for the coefficient of concentration, and so this term was deleted and the analysis was rerun with only the *t* and *tc* terms. For the cross term, *Dtc*, $p = 4 \times 10^{-4}$, showing that the loss of viral titer depended on the concentration on the surface density. The half-life of the viral titer is

$$t_{1/2} = \log 2/(B + Dc) \quad (6)$$

so the significant value of *D* shows that the half-life of SARS-CoV-2 titer decreases with the concentration of Ag_2O in the coating, a major conclusion of this paper. Values of all coefficients are in Table 2.

3.4. Silver Oxide Coatings Kill Bacteria. We tested the Ag_2O-coating and the $2xAg_2O$-coating against three bacteria strains by placing a 10 μL droplet of bacterial cells on the solid and measuring the CFU after a predefined period of time. Figure 5 shows the antibacterial activity of silver oxide coatings against *P. aeruginosa*, *S. aureus*, and MRSA. Both coatings are extremely effective against all three bacteria as demonstrated by the death of bacteria at 1 h. We quantified the efficacy of the coatings using the following equations:

$$\log \mathrm{Survival} = \mathrm{mean}[\log_{10}(\mathrm{sample\ CFU})] - \mathrm{mean}[\log_{10}(\mathrm{input\ CFU})] \quad (7)$$

$$\log \mathit{Reduction} = \mathrm{mean}[\log_{10}(\mathrm{uncoated\ CFU})] - \mathrm{mean}[\log_{10}(\mathrm{coated\ CFU})] \quad (8)$$

$$\%\ \mathrm{Killing} = (1 - 10^{\log \mathrm{Survival}}) \times 100 \quad (9)$$

$$\%\ \mathit{Reduction} = (1 - 10^{-\log \mathit{Reduction}}) \times 100 \quad (10)$$

We use the word survival for simplicity but acknowledge that the CFU assay measures those cells that can reproduce to form a colony. Table 2 lists the survival (in log units) compared to both the input of bacteria, and the *Reduction* compared to glass at 1 h. Both coatings demonstrated excellent antibacterial activity, and the results indicate that the number of viable bacteria was reduced by at least 1.8 log units (>98.7% *Reduction*) on the Ag_2O-coating and at least 2 log units (>99.3% *Reduction*) on the $2xAg_2O$-coating compared to glass in 1 h. Again, the reduction was greater with more Ag_2O present in the film, and there was no significant *Reduction* for TEOS-only coatings (see Figures S10−S12 in Supporting Information), indicating that Ag_2O is the active ingredient.

The significance of time and Ag_2O concentration was again determined by a regression analysis using eq 5 (by replacing TCID_{50} with CFU). Again, the effect of concentration was insignificant and was omitted in subsequent analysis. In common with SARS-CoV-2, the cross term, *tc*, shows that a greater density of Ag_2O in the coating leads to greater inactivation of all three bacteria over time. More precisely, a greater density of Ag_2O in the coating reduces the half-life of the bacteria.

The $2xAg_2O$-coating demonstrated an excellent antibacterial activity by reducing the viable cells of *P. aeruginosa* and MRSA by more than 99.9% ($p = 7 \times 10^{-6}$ and $p = 7 \times 10^{-3}$ respectively) after 1 h, and reducing *S. aureus* by 99.5% ($p = 2 \times 10^{-7}$) after 1 h compared to uncoated glass. The Ag_2O-coating also showed a considerable *Reduction* in comparison to uncoated glass. The *Reduction* of viable *P. aeruginosa*, *S. aureus* and MRSA on this coating was 99.9% ($p = 7 \times 10^{-6}$), 98.3% ($p = 6 \times 10^{-6}$), and 96.4% ($p = 4 \times 10^{-4}$), respectively, compared to uncoated glass after 1 h (Figure 5).

3.5. Ag_2O-coatings Are Transparent and Retain Touch-Screen Function. The Ag_2O-coatings are transparent, with about 60−75% of the transmission of glass in the visible range and only small variation in transmission with color (Figure 6A). As a result, the colors of a smart phone screen are retained when a screen protector with the $2xAg_2O$-coating is attached to a smart phone screen (Figure 6B). Importantly, the screen function is retained with the coating in place (see video in Supporting Information).

3.6. The Antimicrobial Coatings Are Resistant to Abrasion. We also conducted an EPA abrasion test (slightly modified) on the $2xAg_2O$ coating. After abrasion, the antimicrobial properties were unchanged, demonstrating that

https://doi.org/10.1021/acsami.1c20872
ACS Appl. Mater. Interfaces 2022, 14, 8718−8727

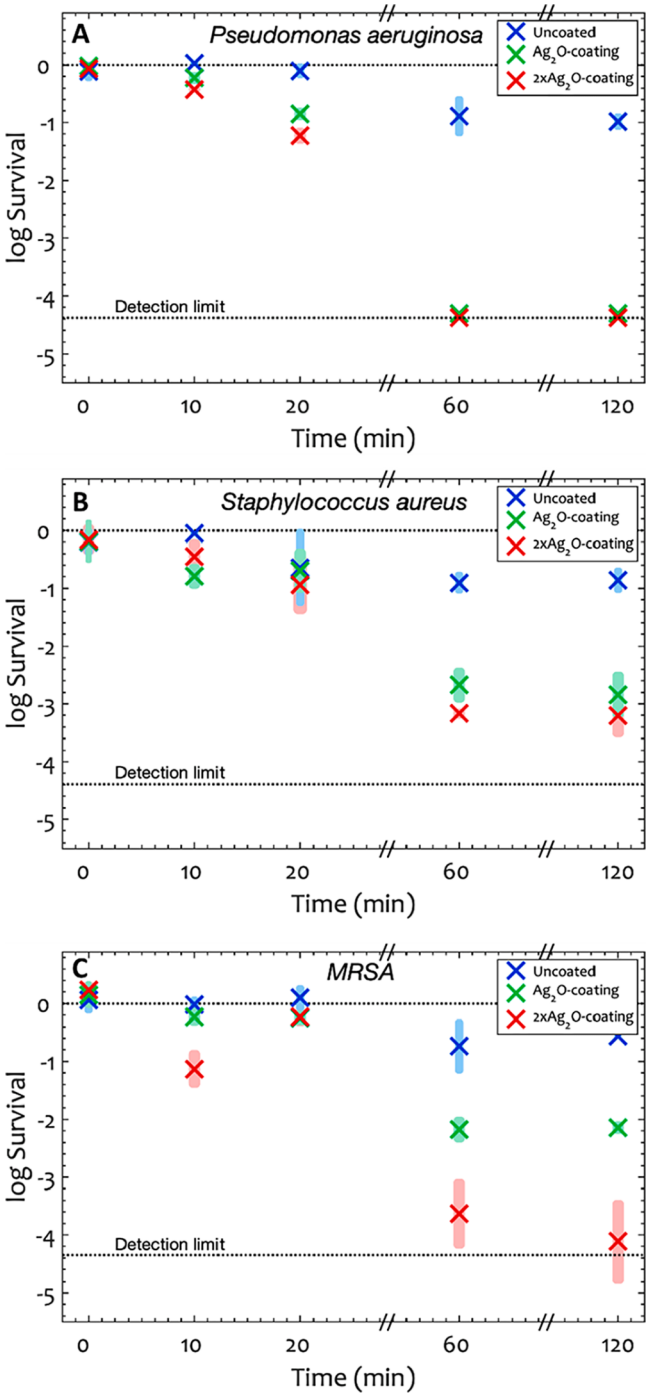

Figure 5. Log survival in colony forming units (eq 1) over time for (A) *P. aeruginosa*, (B) *S. aureus*, and (C) MRSA. Shaded rectangles represent the 95% confidence interval, and × represents the average of the log of the CFU at each time point. The log input titers were 6.08, 6.09, and 6.05 for *P. aeruginosa, S. aureus*, and MRSA respectively. After 1 h, the average killing percentage of *P. aeruginosa, S. aureus*, and MRSA were >99.9% on $2xAg_2O$-coating and >99.3% on Ag_2O-coating. Silver oxide transparent coatings significantly reduced the CFU units of the bacteria compared to uncoated glass (ANOVA $p = 7 \times 10^{-3}$).

the coating was robust (see Figure S13 in Supporting Information).

3.7. Efficacy after Repeated Exposures to Droplets Containing Bacterial Suspension. Although the $2xAg_2O$

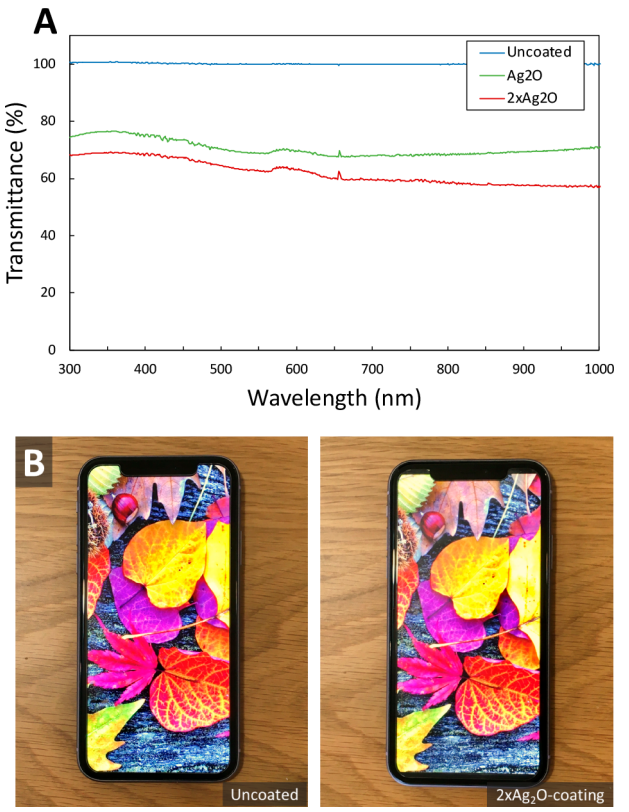

Figure 6. (A) UV−Vis transmission spectrum of glass, Ag_2O-coating, and $2xAg_2O$-coating showing that both films demonstrate more than 60−75% transparency in the visible range (400−700 nm). (B) A smart phone (iPhone 11) with uncoated and $2xAg_2O$-coated screen protector (Mkeke, Amazon B07HRN9J19, tempered glass). The visual appeal and the touch-screen function are retained with the antimicrobial screen protector in place.

coating is very robust against water and ethanol and passes the modified EPA abrasion test, the antibacterial efficacy was diminished after multiple exposures to suspensions of bacteria in droplets. Therefore, we modified the fabrication method to obtain a more robust coating. The principal change was that we increased the amount of silica in the film by increasing the TEOS from 2.8% to 20% (v/v) in ethanol solution. To achieve polymerization of the greater thickness of coating, we increased the time of exposure to the vapor to 60 h and the heat treatment to 75 °C for 40 min. We refer to this modified coating as the M-$2xAg_2O$-coating. The M-$2xAg_2O$-coating was characterized with SEM with XPS (Figure S14), which showed a lower silver content, consistent with some of the silver oxide being covered by the thicker TEOS layer. The visible spectrum showed that the transparency of the $2xAg_2O$-coating was retained (Figure S15).

We tested the antibacterial performance of the M-$2xAg_2O$-coating against *P. aeruginosa* and MRSA (Figure 7). After 1 h, the microbial survival was below the detection limit with >99.99% killing, a 99.80% *Reduction* for *P. aeruginosa* and 99.97% *Reduction* for MRSA compared to the uncoated glass. The results were not statistically different from the $2xAg_2O$-coating at any time point. We then determined the efficacy of this coating after multiple exposures to the microbe, with a series of exposure/bacterial assay/cleaning cycles (see Supporting Information for details). More than 99.9% of *P. aeruginosa* were killed in 1 h after four cycles (see Figure S16 in

https://doi.org/10.1021/acsami.1c20872
ACS Appl. Mater. Interfaces 2022, 14, 8718−8727

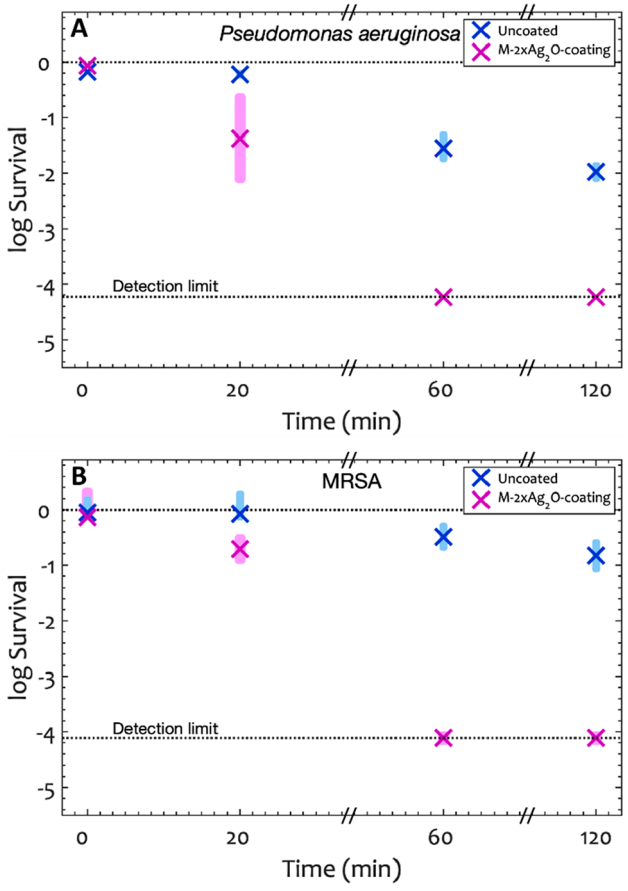

Figure 7. Log survival in colony forming units (eq 6) over time for (A) *P. aeruginosa*, and (B) MRSA on the M-2xAg_2O-coating. Shaded rectangles represent the 95% confidence interval, and × represents the average of the log of the CFU at each time point. The log input titers were 5.93 ± 0.02 for *P. aeruginosa* and 6.05 ± 0.12 for MRSA. After 1 h, the average killing percentage of *P. aeruginosa* and MRSA was 99.99% on the M-2xAg_2O-coating. The antibacterial results on the M-2xAg_2O-coating are not statistically different from the 2xAg_2O-coating results (two tailed, unpaired $p > 0.12$).

Supporting Information). These results show that the coating is still highly active after repeated exposure to the bacteria.

4. DISCUSSION

4.1. Antimicrobial Mechanism of Silver Oxide. The strong antibacterial activity[61−63] of silver oxide has been attributed to silver ion species,[64−66] which have a finite solubility in water ($Ag_2O + H_2O \leftrightarrow 2Ag^+ + 2OH^-$, $pK_s = 7.7$; $Ag_2O + H_2O \leftrightarrow 2Ag(OH)$, $pK_s = 5.7$; $Ag_2O + H_2O + 2OH^- \leftrightarrow 2Ag(OH)_2^-$, $pK_s = 3.7$).[67] The mechanism of action of the silver ions is believed to be either one or a combination of (1) the generation of reactive oxygen species (ROS)[64] and exertion of oxidative stress on cells, and (2) the release and penetration of Ag^+ ions into the microbe and damaging the cell membrane.[65,66] Park et al. reported that the superoxide radical was the major form of the reactive oxygen species generated by silver ions, while H_2O_2 was unlikely to be induced.[68] These reactive oxygen species exert an oxidative stress and damage DNA accordingly which will lead to the killing of bacteria.[69] Silver ions, on the other hand, lead to a loss of cell viability by damaging the cell membrane.[66] Minoshima et al. reported that silver oxide particles damage the viral envelope of influenza A virus and bacteriophage Qβ virus.[70]

There is a possibility that the efficacy of Ag_2O depends on light. If the bandgap of the particles was in the visible range, light could cause the excitation of electrons to the conduction band, which could then act as reducing agents. We compared the antimicrobial efficacy of the 2xAg_2O-coating in visible light and in the dark (see Figure S17 in Supporting Information). A Student's *t* test did not resolve a significant difference between light and dark measurements ($p \gg 0.05$), and therefore the silver oxide coating does not require light for its antimicrobial properties.

5. CONCLUSION

We fabricated two silver oxide in silica coatings, Ag_2O and 2xAg_2O, that inactivate SARS-CoV-2 (95.4% and 99.8% in 1 h) and kill *P. aeruginosa*, (99.99% in 1 h), *S. aureus* (99.78% and 99.93% in 1 h), and the antibiotic-resistant strain MRSA (99.33% and 99.98% in 1 h). The coating was fabricated using a modification of the Stöber method to bind silver oxide particles to a glass substrate. The coated glass is transparent, which means that it does not degrade the aesthetic appeal of materials and it can be applied where transparency is important for function. For example, we showed that when a mobile phone screen was coated, both the screen clarity and the function of the touch-screen were retained. The combination of transparency and antimicrobial action means that the coating should find application for multiuser touch-screens, such as check-out facilities in grocery stores.

■ ASSOCIATED CONTENT

Supporting Information

The Supporting Information is available free of charge at https://pubs.acs.org/doi/10.1021/acsami.1c20872.

Synthesized particle size distribution (Figure S1). AFM images of 2xAg_2O coating (Figure S2). Surface elemental analysis of coatings by EDS (Table S1). SEM images of uncoated glass and TEOS-coated glass (Figure S3). Time lapse of the sol−gel reaction (Figure S4). The effect of ammonia on the morphology of silver oxide particles (Figure S5). The effect of heat treatment on the morphology of silver oxide particles (Figure S6). Contact angle images of silver oxide coatings (Figure S7). Test of attachment of particles using ultrasonication (Figure S8). The comparison of SARS-CoV-2 titer log($TCID_{50}$/mL) data on TEOS and glass over time (Figure S9). The comparison of log survival of *P. aeruginosa* on TEOS and glass over time (Figure S10). The comparison of log survival of *S. aureus* on TEOS and glass over time (Figure S11). The comparison of log survival of MRSA on TEOS and glass over time (Figure S12). The effect of abrasion in the antibacterial properties of the silver oxide coating (Figure S13). Characterization of the M-2xAg_2O-coating (Figure S14). UV−Vis transmission spectrum of uncoated glass and the M-2xAg2O-coating (Figure S15). The effect of multiple bacteria exposure/sonicating/vortexing/titration/cleaning on the M-2xAg2O coating (Figure S16). The effect of absence of light in the antibacterial properties of silver oxide coating (Figure S17). SARS-CoV-2 $TCID_{50}$/mL assay results for Figure 4 (Table S2). *Pseudomonas aeruginosa* CFU assay results for Figure 5 (Table S3). *Staphylococcus aureus* CFU assay results for Figure 5 (Table S4). MRSA CFU assay results

https://doi.org/10.1021/acsami.1c20872
ACS Appl. Mater. Interfaces 2022, 14, 8718−8727

for Figure 5 (Table S5). *P. aeruginosa* CFU assay results for Figure 7 (Table S6). MRSA CFU assay results for Figure 7 (Table S7). *P. aeruginosa* CFU assay results for Figure S13 (Table S8). *P. aeruginosa* CFU assays results for Figure S17 (Table S9). MRSA CFU assays results for Figure S17 (Table S10) (PDF)

Retention of screen function with the coating in place (MOV)

AUTHOR INFORMATION

Corresponding Authors

Leo L. M. Poon − *School of Public Health, LKS Faculty of Medicine, The University of Hong Kong, Hong Kong Special Administrative Region, Hong Kong, China; Centre for Immunity and Infection, Hong Kong Science Park, Hong Kong, Hong Kong, China; HKU-Pasteur Research Pole, LKS Faculty of Medicine, The University of Hong Kong, Hong Kong, China*; Email: llmpoon@hku.hk

William A. Ducker − *Department of Chemical Engineering and Center for Soft Matter and Biological Physics, Virginia Tech, Blacksburg, Virginia 24061, United States*; orcid.org/0000-0002-8207-768X; Email: wducker@vt.edu

Authors

Mohsen Hosseini − *Department of Chemical Engineering and Center for Soft Matter and Biological Physics, Virginia Tech, Blacksburg, Virginia 24061, United States*; orcid.org/0000-0002-9482-0215

Alex W. H. Chin − *School of Public Health, LKS Faculty of Medicine, The University of Hong Kong, Hong Kong Special Administrative Region, Hong Kong, China; Centre for Immunity and Infection, Hong Kong Science Park, Hong Kong, Hong Kong, China*; orcid.org/0000-0002-6556-9092

Myra D. Williams − *Department of Biological Sciences, Virginia Tech, Blacksburg, Virginia 24061, United States*

Saeed Behzadinasab − *Department of Chemical Engineering and Center for Soft Matter and Biological Physics, Virginia Tech, Blacksburg, Virginia 24061, United States*; orcid.org/0000-0002-6271-2623

Joseph O. Falkinham, III − *Department of Biological Sciences, Virginia Tech, Blacksburg, Virginia 24061, United States*

Complete contact information is available at: https://pubs.acs.org/10.1021/acsami.1c20872

Notes

The authors declare the following competing financial interest(s): W.D. declares part ownership in a startup company that intends to produce surface coatings. The other authors declare no conflict of interest.

ACKNOWLEDGMENTS

The authors thank Stephen McCartney for assisting in capturing a part of the SEM images and acknowledge the use of Electron Microscopy facilities and the X-ray diffraction machine within the Nanoscale Characterization and Fabrication Laboratory and Material Characterization Laboratory at Virginia Polytechnic Institute and State University. We also thank Xu Feng for capturing the XPS spectra and acknowledge the use of Surface Analysis Laboratory in Department of Chemistry at Virginia Tech, which is supported by the National Science Foundation under grant no. CHE-1531834. This work was supported by the National Science Foundation under grant no. CBET-1902364, the Health and Medical Research Fund (COVID190116), and the National Institute of Allergy and Infectious Diseases (contract HHSN272201400006C).

REFERENCES

(1) Andersen, B. M. Microbes, Transmission Routes and Survival Outside the Body. In *Prevention and Control of Infections in Hospitals*; Springer, 2019; pp 23−28.

(2) Antonovics, J.; Wilson, A. J.; Forbes, M. R.; Hauffe, H. C.; Kallio, E. R.; Leggett, H. C.; Longdon, B.; Okamura, B.; Sait, S. M.; Webster, J. P. The Evolution of Transmission Mode. *Philosophical Transactions of the Royal Society B: Biological Sciences* **2017**, *372* (1719), 20160083.

(3) Weiner, L. M.; Webb, A. K.; Limbago, B.; Dudeck, M. A.; Patel, J.; Kallen, A. J.; Edwards, J. R.; Sievert, D. M. Antimicrobial-resistant Pathogens Associated with Healthcare-associated Infections: Summary of Data Reported to the National Healthcare Safety Network at the Centers for Disease Control and Prevention, 2011−2014. *Infection Control & Hospital Epidemiology* **2016**, *37* (11), 1288−1301.

(4) Solberg, C. O. Spread of Staphylococcus aureus in Hospitals: Causes and Prevention. *Scandinavian Journal of Infectious Diseases* **2000**, *32* (6), 587−595.

(5) Xiao, S.; Jones, R. M.; Zhao, P.; Li, Y. The Dynamic Fomite Transmission of Methicillin-resistant Staphylococcus aureus in Hospitals and the Possible Improved Intervention Methods. *Building and Environment* **2019**, *161*, 106246.

(6) Davis, K. A.; Stewart, J. J.; Crouch, H. K.; Florez, C. E.; Hospenthal, D. R. Methicillin-resistant Staphylococcus aureus (MRSA) Nares Colonization at Hospital Admission and Its Effect on Subsequent MRSA Infection. *Clinical Infectious Diseases* **2004**, *39* (6), 776−782.

(7) Harris, S. R.; Feil, E. J.; Holden, M. T.; Quail, M. A.; Nickerson, E. K.; Chantratita, N.; Gardete, S.; Tavares, A.; Day, N.; Lindsay, J. A.; et al. Evolution of MRSA During Hospital Transmission and Intercontinental Spread. *Science* **2010**, *327* (5964), 469−474.

(8) Page, K.; Wilson, M.; Parkin, I. P. Antimicrobial Surfaces and Their Potential in Reducing the Role of the Inanimate Environment in the Incidence of Hospital-acquired Infections. *J. Mater. Chem.* **2009**, *19* (23), 3819−3831.

(9) Desai, R.; Pannaraj, P. S.; Agopian, J.; Sugar, C. A.; Liu, G. Y.; Miller, L. G. Survival and Transmission of Community-Associated Methicillin-resistant Staphylococcus aureus from Fomites. *American Journal of Infection Control* **2011**, *39* (3), 219−225.

(10) COVID-19 Dashboard by the Center for Systems Science and Engineering (CSSE) at Johns Hopkins University (JHU). Johns Hopkins University, 2020. https://coronavirus.jhu.edu/map.html (accessed December 27, 2021).

(11) Coutard, B.; Valle, C.; de Lamballerie, X.; Canard, B.; Seidah, N.; Decroly, E. The Spike Glycoprotein of The New Coronavirus 2019-nCoV Contains A Furin-Like Cleavage Site Absent in Cov of The Same Clade. *Antiviral Research* **2020**, *176*, 104742.

(12) Prather, K. A.; Wang, C. C.; Schooley, R. T. Reducing Transmission of SARS-CoV-2. *Science* **2020**, *368* (6498), 1422−1424.

(13) Sia, S. F.; Yan, L.-M.; Chin, A. W.; Fung, K.; Choy, K.-T.; Wong, A. Y.; Kaewpreedee, P.; Perera, R. A.; Poon, L. L.; Nicholls, J. M.; et al. Pathogenesis and Transmission of SARS-CoV-2 in Golden Hamsters. *Nature* **2020**, *583* (7818), 834−838.

(14) Meiksin, A. Dynamics of COVID-19 Transmission Including Indirect Transmission Mechanisms: A Mathematical Analysis. *Epidemiology & Infection* **2020**, *148*, No. e257.

(15) Harbourt, D. E.; Haddow, A. D.; Piper, A. E.; Bloomfield, H.; Kearney, B. J.; Fetterer, D.; Gibson, K.; Minogue, T. Modeling the Stability of Severe Acute Respiratory Syndrome Coronavirus 2 (SARS-CoV-2) on Skin, Currency, and Clothing. *PLoS Neglected Tropical Diseases* **2020**, *14* (11), No. e0008831.

(16) Cromer, A. L.; Latham, S. C.; Bryant, K. G.; Hutsell, S.; Gansauer, L.; Bendyk, H. A.; Steed, R.; Carney, M. C. Monitoring and Feedback of Hand Hygiene Compliance and the Impact on Facility-acquired Methicillin-resistant Staphylococcus aureus. *American Journal of Infection Control* **2008**, *36* (9), 672−677.
(17) Bhalla, A.; Pultz, N. J.; Gries, D. M.; Ray, A. J.; Eckstein, E. C.; Aron, D. C.; Donskey, C. J. Acquisition of Nosocomial Pathogens on Hands After Contact with Environmental Surfaces Near Hospitalized Patients. *Infection Control & Hospital Epidemiology* **2004**, *25* (2), 164−167.
(18) Lei, H.; Xiao, S.; Cowling, B. J.; Li, Y. Hand Hygiene and Surface Cleaning Should Be Paired for Prevention of Fomite Transmission. *Indoor Air* **2020**, *30* (1), 49−59.
(19) Lei, H.; Jones, R. M.; Li, Y. Exploring Surface Cleaning Strategies in Hospital to Prevent Contact Transmission of Methicillin-resistant Staphylococcus aureus. *BMC Infectious Diseases* **2017**, *17* (1), 1−9.
(20) Monge, F. A.; Jagadesan, P.; Bondu, V.; Donabedian, P. L.; Ista, L.; Chi, E. Y.; Schanze, K. S.; Whitten, D. G.; Kell, A. M. Highly Effective Inactivation of SARS-CoV-2 by Conjugated Polymers and Oligomers. *ACS Appl. Mater. Interfaces* **2020**, *12* (50), 55688−55695.
(21) Hosseini, M.; Behzadinasab, S.; Benmamoun, Z.; Ducker, W. A. The Viability of SARS-COV-2 on Solid Surfaces. *Curr. Opin. Colloid Interface Sci.* **2021**, *55*, 101481.
(22) Van Doremalen, N.; Bushmaker, T.; Morris, D. H.; Holbrook, M. G.; Gamble, A.; Williamson, B. N.; Tamin, A.; Harcourt, J. L.; Thornburg, N. J.; Gerber, S. I.; et al. Aerosol and Surface Stability of SARS-CoV-2 as Compared with SARS-CoV-1. *New England Journal of Medicine* **2020**, *382* (16), 1564−1567.
(23) Chin, A. W.; Chu, J. T.; Perera, M. R.; Hui, K. P.; Yen, H.-L.; Chan, M. C.; Peiris, M.; Poon, L. L. Stability of SARS-CoV-2 in Different Environmental Conditions. *Lancet Microbe* **2020**, *1* (1), No. e10.
(24) Kramer, A.; Schwebke, I.; Kampf, G. How long do nosocomial pathogens persist on inanimate surfaces? A systematic review. *BMC Infectious Diseases* **2006**, *6* (1), 1−8.
(25) Williams, C.; Davis, D. L. Methicillin-resistant Staphylococcus aureus fomite survival. *American Society for Clinical Laboratory Science* **2009**, *22* (1), 34−38.
(26) Yuan, W.; Ji, J.; Fu, J.; Shen, J. A Facile Method to Construct Hybrid Multilayered Films as A Strong and Multifunctional Antibacterial Coating. *Journal of Biomedical Materials Research Part B: Applied Biomaterials* **2008**, *85* (2), 556−563.
(27) Behzadinasab, S.; Chin, A. W. H.; Hosseini, M.; Poon, L. L. M.; Ducker, W. A. SARS-CoV-2 virus transfers to skin through contact with contaminated solids. *Scientific Reports* **2021**, *2021* (11), 22868.
(28) Rakowska, P. D.; Tiddia, M.; Faruqui, N.; Bankier, C.; Pei, Y.; Pollard, A. J.; Zhang, J.; Gilmore, I. S. Antiviral Surfaces and Coatings and Their Mechanisms of Action. *Commun. Mater.* **2021**, *2* (1), 1−19.
(29) Behzadinasab, S.; Chin, A.; Hosseini, M.; Poon, L. L.; Ducker, W. A. A Surface Coating that Rapidly Inactivates SARS-CoV-2. *ACS Appl. Mater. Interfaces* **2020**, *12* (31), 34723−34727.
(30) Hosseini, M.; Chin, A. W.; Behzadinasab, S.; Poon, L. L.; Ducker, W. A. Cupric Oxide Coating That Rapidly Reduces Infection by SARS-CoV-2 via Solids. *ACS Appl. Mater. Interfaces* **2021**, *13* (5), 5919−5928.
(31) Hutasoit, N.; Kennedy, B.; Hamilton, S.; Luttick, A.; Rahman Rashid, R. A.; Palanisamy, S. SARS-CoV-2 (COVID-19) Inactivation Capability of Copper-Coated Touch Surface Fabricated by Cold-Spray Technology. *Manufacturing Letters* **2020**, *25*, 93−97.
(32) Hosseini, M.; Behzadinasab, S.; Chin, A. W.; Poon, L. L.; Ducker, W. A. Reduction of Infectivity of SARS-CoV-2 by Zinc Oxide Coatings. *ACS Biomaterials Science & Engineering* **2021**, *7* (11), 5022−5027.
(33) Olsen, M.; Campos, M.; Lohning, A.; Jones, P.; Legget, J.; Bannach-Brown, A.; McKirdy, S.; Alghafri, R.; Tajouri, L. Mobile Phones Represent A Pathway for Microbial Transmission: A Scoping Review. *Travel Medicine and Infectious Disease* **2020**, *35*, 101704.
(34) Karabay, O.; Koçoglu, E.; Tahtaci, M. The Role of Mobile Phones in the Spread of Bacteria Associated with Nosocomial Infections. *J. Infect Dev Ctries* **2007**, *1* (1), 72−73.
(35) Deusenbery, C.; Wang, Y.; Shukla, A. Recent Innovations in Bacterial Infection Detection and Treatment. *ACS Infectious Diseases* **2021**, *7* (4), 695−720.
(36) Behzadinasab, S.; Williams, M. D.; Hosseini, M.; Poon, L. L. M.; Chin, A. W. H.; Falkinham, J. O.; Ducker, W. A. Transparent and Sprayable Surface Coatings that Kill Drug-Resistant Bacteria Within Minutes and Inactivate SARS- CoV-2 Virus. *ACS Appl. Mater. Interfaces* **2021**, *13* (46), 54706−54714.
(37) Salwiczek, M.; Qu, Y.; Gardiner, J.; Strugnell, R. A.; Lithgow, T.; McLean, K. M.; Thissen, H. Emerging Rules for Effective Antimicrobial Coatings. *Trends Biotechnol.* **2014**, *32* (2), 82−90.
(38) Cloutier, M.; Mantovani, D.; Rosei, F. Antibacterial Coatings: Challenges, Perspectives, and Opportunities. *Trends Biotechnol.* **2015**, *33* (11), 637−652.
(39) Akiyama, T.; Miyamoto, H.; Yonekura, Y.; Tsukamoto, M.; Ando, Y.; Noda, I.; Sonohata, M.; Mawatari, M. Silver Oxide-containing Hydroxyapatite Coating Has in vivo Antibacterial Activity in the Rat Tibia. *Journal of Orthopaedic Research* **2013**, *31* (8), 1195−1200.
(40) Johnson, J. R.; Roberts, P. L.; Olsen, R. J.; Moyer, K. A.; Stamm, W. E. Prevention of Catheter-associated Urinary Tract Infection with A Silver Oxide-coated Urinary Catheter: Clinical and Microbiologic Correlates. *Journal of Infectious Diseases* **1990**, *162* (5), 1145−1150.
(41) Babu, P. J.; Doble, M.; Raichur, A. M. Silver Oxide Nanoparticles Embedded Silk Fibroin Spuns: Microwave Mediated Preparation, Characterization and Their Synergistic Wound Healing and Anti-bacterial Activity. *J. Colloid Interface Sci.* **2018**, *513*, 62−71.
(42) Shahrbabak, M. S. N.; Sharifianjazi, F.; Rahban, D.; Salimi, A. A Comparative Investigation on Bioactivity and Antibacterial Properties of Sol-gel Derived 58S Bioactive Glass Substituted by Ag and Zn. *Silicon* **2019**, *11* (6), 2741−2751.
(43) Manikandan, V.; Velmurugan, P.; Park, J.-H.; Chang, W.-S.; Park, Y.-J.; Jayanthi, P.; Cho, M.; Oh, B.-T. Green Synthesis of Silver Oxide Nanoparticles and Its Antibacterial Activity Against Dental Pathogens. *3 Biotech* **2017**, *7* (1), 72.
(44) Kim, M. H.; Park, H.; Nam, H. C.; Park, S. R.; Jung, J.-Y.; Park, W. H. Injectable Methylcellulose Hydrogel Containing Silver Oxide Nanoparticles for Burn Wound Healing. *Carbohydr. Polym.* **2018**, *181*, 579−586.
(45) Fakhri, A.; Tahami, S.; Nejad, P. A. Preparation and Characterization of Fe_3O_4-Ag_2O Quantum Dots Decorated Cellulose Nanofibers as A Carrier of Anticancer Drugs for Skin Cancer. *Journal of Photochemistry and Photobiology B: Biology* **2017**, *175*, 83−88.
(46) Vu, A. A.; Robertson, S. F.; Ke, D.; Bandyopadhyay, A.; Bose, S. Mechanical and Biological Properties of ZnO, SiO_2, and Ag_2O Doped Plasma Sprayed Hydroxyapatite Coating for Orthopaedic and Dental Applications. *Acta Biomaterialia* **2019**, *92*, 325−335.
(47) Hench, L. L.; West, J. K. The Sol-gel Process. *Chem. Rev.* **1990**, *90* (1), 33−72.
(48) Ghimire, P. P.; Jaroniec, M. Renaissance of Stöber Method for Synthesis of Colloidal Particles: New Developments and Opportunities. *J. Colloid Interface Sci.* **2021**, *584*, 838−865.
(49) Stöber, W.; Fink, A.; Bohn, E. Controlled Growth of Monodisperse Silica Spheres in The Micron Size Range. *J. Colloid Interface Sci.* **1968**, *26* (1), 62−69.
(50) Chang, Y.-R.; Taylor, S.; Duncan, S.; Mazilu, D. A.; Ritter, A.; Ducker, W. A. Fabrication of Stabilized Colloidal Crystal Monolayers. *Colloids Surf., A* **2017**, *514*, 185−191.
(51) Chen, Y.-J.; Chiang, Y.-W.; Huang, M. H. Synthesis of Diverse Ag_2O Crystals and Their Facet-Dependent Photocatalytic Activity Examination. *ACS Appl. Mater. Interfaces* **2016**, *8* (30), 19672−19679.
(52) Wang, X.; Wu, H.-F.; Kuang, Q.; Huang, R.-B.; Xie, Z.-X.; Zheng, L.-S. Shape-dependent Antibacterial Activities of Ag_2O Polyhedral Particles. *Langmuir* **2010**, *26* (4), 2774−2778.

https://doi.org/10.1021/acsami.1c20872
ACS Appl. Mater. Interfaces 2022, 14, 8718−8727

(53) Rabani, E.; Reichman, D. R.; Geissler, P. L.; Brus, L. E. Drying-mediated Self-assembly of Nanoparticles. *Nature* **2003**, *426* (6964), 271−274.
(54) Grosso, D.; Cagnol, F.; Soler-Illia, G. d. A.; Crepaldi, E. L.; Amenitsch, H.; Brunet-Bruneau, A.; Bourgeois, A.; Sanchez, C. Fundamentals of Mesostructuring Through Evaporation-induced Self-assembly. *Adv. Funct. Mater.* **2004**, *14* (4), 309−322.
(55) Malenovska, H. Virus Quantitation by Transmission Electron Microscopy, TCID50, and the Role of Timing Virus Harvesting: A Case Study of Three Animal Viruses. *J. Virol. Methods* **2013**, *191* (2), 136−140.
(56) Chan, K.; Lai, S.; Poon, L.; Guan, Y.; Yuen, K.; Peiris, J. Analytical Sensitivity of Rapid Influenza Antigen Detection Tests for Swine-origin Influenza Virus (H1N1). *J. Clin. Virol.* **2009**, *45* (3), 205−207.
(57) Reed, L. J.; Muench, H. A Simple Method of Estimating Fifty Percent Endpoints. *American Journal of Epidemiology* **1938**, *27* (3), 493−497.
(58) Interim Method for Evaluating the Efficacy of Antimicrobial Surface Coatings. EPA. 10/2/2020. https://www.epa.gov/pesticide-analytical-methods/antimicrobial-testing-methods-procedures-interim-method-evaluating (accessed August 25, 2021).
(59) Britton, H.; Williams, W. G. Electrometric Studies of The Precipitation of Hydroxides. Part XIII. The Constitution of Aqueous Solutions of Silver Oxide in Ammonia, mono-, di-, and tri-methylamine and-ethylamine, Pyridine And Ethylenediamine; with A Note on the Dissociation Constants of The Amines. *Journal of the Chemical Society (Resumed)* **1935**, 796−801.
(60) Johnston, H. L.; Cuta, F.; Garrett, A. B. The Solubility of Silver Oxide in Water, in Alkali And in Alkaline Salt Solutions. The Amphoteric Character of Silver Hydroxide. *J. Am. Chem. Soc.* **1933**, *55* (6), 2311−2325.
(61) Allahverdiyev, A. M.; Abamor, E. S.; Bagirova, M.; Rafailovich, M. Antimicrobial Effects of TiO_2 And Ag_2O Nanoparticles Against Drug-resistant Bacteria and Leishmania Parasites. *Future Microbiology* **2011**, *6* (8), 933−940.
(62) Negi, H.; Rathinavelu Saravanan, P.; Agarwal, T.; Ghulam Haider Zaidi, M.; Goel, R. In Vitro Assessment of Ag_2O Nanoparticles Toxicity Against Gram-positive and Gram-negative Bacteria. *Journal of General and Applied Microbiology* **2013**, *59* (1), 83−88.
(63) Rokade, A. A.; Patil, M. P.; Yoo, S. I.; Lee, W. K.; Park, S. S. Pure Green Chemical Approach for Synthesis of Ag_2O Nanoparticles. *Green Chemistry Letters and Reviews* **2016**, *9* (4), 216−222.
(64) Rajabi, A.; Ghazali, M. J.; Mahmoudi, E.; Baghdadi, A. H.; Mohammad, A. W.; Mustafah, N. M.; Ohnmar, H.; Naicker, A. S. Synthesis, Characterization, and Antibacterial Activity of Ag_2O-loaded Polyethylene Terephthalate Fabric via Ultrasonic Method. *Nanomaterials* **2019**, *9* (3), 450.
(65) Bellantone, M.; Williams, H. D.; Hench, L. L. Broad-spectrum Bactericidal Activity of Ag_2O-doped Bioactive Glass. *Antimicrob. Agents Chemother.* **2002**, *46* (6), 1940−1945.
(66) Li, D.; Chen, S.; Zhang, K.; Gao, N.; Zhang, M.; Albasher, G.; Shi, J.; Wang, C. The Interaction of Ag_2O Nanoparticles with Escherichia coli: Inhibition-sterilization Process. *Sci. Rep.* **2021**, *11* (1), 1−9.
(67) Feitknecht, W.; Schindler, P. Solubility Constants of Metal Oxides, Metal Hydroxides and Metal Hydroxide Salts in Aqueous Solution. *Pure Appl. Chem.* **1963**, *6* (2), 125−206.
(68) Park, H.-J.; Kim, J. Y.; Kim, J.; Lee, J.-H.; Hahn, J.-S.; Gu, M. B.; Yoon, J. Silver-ion-mediated Reactive Oxygen Species Generation Affecting Bactericidal Activity. *Water Research* **2009**, *43* (4), 1027−1032.
(69) Makvandi, P.; Wang, C. y.; Zare, E. N.; Borzacchiello, A.; Niu, L. n.; Tay, F. R. Metal-based Nanomaterials in Biomedical Applications: Antimicrobial Activity and Cytotoxicity Aspects. *Adv. Funct. Mater.* **2020**, *30* (22), 1910021.
(70) Minoshima, M.; Lu, Y.; Kimura, T.; Nakano, R.; Ishiguro, H.; Kubota, Y.; Hashimoto, K.; Sunada, K. Comparison of The Antiviral Effect of Solid-State Copper and Silver Compounds. *Journal of Hazardous Materials* **2016**, *312*, 1−7.

https://doi.org/10.1021/acsami.1c20872
ACS Appl. Mater. Interfaces 2022, 14, 8718−8727